Hepatocytes release ceramide-enriched pro-inflammatory extracellular vesicles in an IRE1α-dependent manner[s]

Eiji Kakazu,[*,†] **Amy S. Mauer,**[*] **Meng Yin,**[§] **and Harmeet Malhi**[1,*]

Division of Gastroenterology and Hepatology[*] and Department of Radiology,[§] Mayo Clinic, Rochester, MN 55905; and Department of Community Medical Supports,[†] Tohoku Medical Megabank Organization, Tohoku University, Aobaku, Sendai, 980-8573 Japan

Abstract Nonalcoholic steatohepatitis (NASH) is a lipotoxic disease wherein activation of endoplasmic reticulum (ER) stress response and macrophage-mediated hepatic inflammation are key pathogenic features. However, the lipid mediators linking these two observations remain elusive. We postulated that ER stress-regulated release of pro-inflammatory extracellular vesicles (EVs) from lipotoxic hepatocytes may be this link. EVs were isolated from cell culture supernatants of hepatocytes treated with palmitate (PA) to induce lipotoxic ER stress, characterized by immunofluorescence, Western blotting, electron microscopy, and nanoparticle tracking analysis. Sphingolipids were measured by tandem mass spectrometry. EVs were employed in macrophage chemotaxis assays. PA induced significant EV release. Because PA activates ER stress, we used KO hepatocytes to demonstrate that PA-induced EV release was mediated by inositol requiring enzyme 1α (IRE1α)/X-box binding protein-1. PA-induced EVs were enriched in C16:0 ceramide in an IRE1α-dependent manner, and activated macrophage chemotaxis via formation of sphingosine-1-phosphate (S1P) from C16:0 ceramide. This chemotaxis was blocked by sphingosine kinase inhibitors and S1P receptor inhibitors. Lastly, elevated circulating EVs in experimental and human NASH demonstrated increased C16:0 ceramide.[Jlr] PA induces C16:0 ceramide-enriched EV release in an IRE1α-dependent manner. The ceramide metabolite, S1P, activates macrophage chemotaxis, a potential mechanism for the recruitment of macrophages to the liver under lipotoxic conditions.—Kakazu, E., A. S. Mauer, M. Yin, and H. Malhi. **Hepatocytes release ceramide-enriched pro-inflammatory extracellular vesicles in an IRE1α-dependent manner.** *J. Lipid Res.* **2016.** 57: 233–245.

Nonalcoholic fatty liver disease (NAFLD, defined by the presence of isolated hepatocellular steatosis) and nonalcoholic steatohepatitis (NASH, defined by the presence of hepatocellular steatosis plus liver inflammation and fibrosis) constitute the spectrum of obesity-associated liver diseases, the most prevalent chronic liver diseases in the Western world (1). NASH patients are at risk for progressive liver fibrosis, which can culminate in cirrhosis with its attendant risks of hepatocellular carcinoma and liver failure. Besides weight loss, there are no effective regulatory agency-approved pharmacologic therapies for NASH (2). Therefore, understanding NASH pathogenesis to facilitate rational drug development is an urgent unmet need.

Circulating and hepatic saturated free fatty acid levels, especially palmitate (PA), are elevated in the obese insulin-resistant state and in NAFLD (3). PA, both directly and indirectly, as a precursor for other toxic lipid moieties such as lysophosphatidyl choline, can activate the apoptotic machinery in hepatocytes (4, 5). PA is also a precursor for ceramide biosynthesis via the de novo pathway. Ceramides are bioactive lipids that are the backbone for

---

sphingolipid synthesis and important structural components of eukaryotic cell membranes (6). They also play important roles in signaling. In the context of obesity-associated disorders, ceramides are known to accumulate in adipose tissues, and the inhibition of ceramide accumulation ameliorates diabetes and atherosclerosis in lipotoxic disorders (6, 7). Recent studies have implicated hepatic C16:0 ceramide accumulation in the pathogenesis of insulin resistance and NASH (8, 9). However, the exact pathways by which C16:0 ceramides mediate liver injury and inflammation remain incompletely defined.

Extracellular vesicles (EVs) are cell-derived membrane-defined circulating nano-particles that are shed both basally and under stress conditions (10). EVs are heterogeneous and composed of particles shed by different mechanisms and of variable sizes. Depending on these characteristics, they can be further classified into exosomes, microparticles, oncosomes, etc. Until advancements permit distinction between these particle types, the all-encompassing term, EV, is most appropriate. EVs are a route for cell-derived cargo to be shed from cells, and a mechanism for delivery of specific cargoes from donor cells to recipient cells, thus acting as carriers of a stress-stimulated message. Recently, studies have demonstrated an increase in circulating EV release under in vitro lipotoxic conditions, circulating EVs in mouse models of NASH and ischemia/reperfusion injury, and in patients with chronic hepatitis C and NASH (11–13). Furthermore, it has been reported that ceramides are needed for the formation of EVs via the multivesicular body (MVB) endosomal trafficking pathway (14). However, whether PA-induced ceramide biosynthesis drives an EV release response is not known.

Hepatocytes are enriched in the endoplasmic reticulum (ER), a membrane-bound organelle that serves as the subcellular site for lipid and sterol synthesis, as well as the folding factory for secreted proteins (15). Perturbations in ER function result in ER stress. ER stress is observed in NAFLD and PA-induced lipotoxicity (15, 16). Indeed, PA can directly activate all three ER stress sensors: *i*) inositol requiring enzyme 1α (IRE1α); *ii*) activating transcription factor 6α (ATF6α); and *iii*) protein kinase-like ER kinase (PERK). Because PA-driven de novo ceramide synthesis occurs at the ER, we asked whether PA-induced lipotoxic ER stress would lead to an EV response, and whether any of the three ER stress sensors would mediate PA-induced EV release.

Although a full spectrum of inflammatory cells exists in the injured liver, macrophages have received the most attention in NASH, as they are recruited to the liver during lipotoxicity (17). Furthermore, inhibition of macrophage activation, recruitment, or accumulation in the liver ameliorates steatohepatitis (16). Herein, we report that PA-induced ER stress leads to EV release. Furthermore, ceramides are enriched in PA-induced EVs, and this phenomenon occurs in an IRE1α-dependent manner. The ceramide-enriched vesicles also contain sphingosine-1-phosphate (S1P), a known inflammatory mediator and activator of macrophages. We speculate that inhibition of

this pathway and/or S1P signaling may be salubrious in NASH.

MATERIALS AND METHODS

Cells

Previously described immortalized mouse hepatocyte (IMH) cell lines derived from IRE1α KO and WT mice (18), ATF6α-WT and KO IMH cell lines, and eIF2α S51A phosphorylation resistant (AA) and WT (SS) IMH cell lines were a kind gift of Dr. Randal Kaufman. The IMH cell lines were cultured in DMEM (Life Technologies) supplemented with 10% FBS, penicillin, and streptomycin. Huh7 cells were cultured in DMEM supplemented with 10% FBS, penicillin, and streptomycin. Primary mouse hepatocytes were isolated by collagenase perfusion followed by Percoll purification, cultured as previously described by us (19), and used in experiments if viability exceeded 95%. For EV isolation, cells were cultured in growth medium supplemented with 5% EV-depleted FBS [prepared by overnight centrifugation at 100,000 *g* at 4°C according to standard protocols (20)] and 1% BSA, with the addition of either PA or oleate (OA) as previously described by us (4), thapsigargin (Tg), or vehicle, respectively. Bone marrow-derived macrophages (BMDMφs) were isolated from the long leg bones of C57Bl/6J mice, as previously described by us (16). Briefly, dissected long bones were flushed with serum-free RPMI and cells were differentiated in 20% L929 cell conditioned medium containing RPMI and used on day 7 after differentiation.

EV isolation

Cells were grown to 90% confluency on 150 mm tissue culture plastic dishes. Before treating, cells were washed twice with PBS and then the medium was changed to assay medium supplemented with PA, OA, or Tg (4). After 14–16 h, supernatant was recovered and sequential low-speed centrifugation was performed to deplete cells and cellular debris at 2,000 *g* for 20 min followed by 20,000 *g* for 30 min (20). The supernatant was further ultracentrifuged at 100,000 *g* for 90 min to pellet EVs, which were washed once by resuspending in PBS followed by ultracentrifugation at 100,000 *g* for 90 min. The final EV pellet was resuspended in PBS and either used for downstream experiments or stored at −80°C. For each experimental condition, isolated EVs were normalized to cell number and expressed relative to the vehicle-treated condition, unless indicated otherwise. Circulating vesicles were isolated from platelet-poor plasma by differential ultracentrifugation, as previously described (20). For human plasma samples, 900 μl each were used. For mouse plasma samples, 100 μl each were used. Briefly, plasma was diluted with an equal volume of PBS and centrifuged at 2,000 *g* for 30 min at 4°C. The clear supernatant was transferred to new tubes and centrifuged at 12,000 *g* for 30 min at 4°C. EVs were isolated from the second spin supernatant by ultracentrifugation at 110,000 *g* for 120 min. Isolated vesicles were characterized by nanoparticle tracking analysis and stored frozen until further analyses.

Nanoparticle tracking analysis

The Nanosight NTA NS300 (Malvern Instruments, UK) equipped with a fast video capture and nanoparticle tracking analysis (NTA) software was used to characterize EV particle size and concentration (21). The instrument was calibrated according to the manufacturer's protocol. EV samples were diluted in PBS to perform measurements in the linear dynamic range of the instrument (2E+08 to 8E+08 particles/ml). Each sample was

perfused through the sample chamber at a constant rate of 25 µl/min using a syringe pump. The light scatter and Brownian motion of each sample of nanoparticles was recorded at least three times, 30 s each at constant room temperature (22.5°C); particle tracks were analyzed by NanoSight software to measure the concentration of the particles (particles per milliliter) and size (in nanometers).

Lipidomics

Ceramides and nonesterified fatty acids were measured using mass spectrometry at the Mayo Clinic Metabolomics Core Laboratory. Briefly, ceramides were extracted from EVs or cell pellets suspended in 1× PBS after the addition of internal standards and sonication. The extracts were measured against a standard curve on the Thermo TSQ Quantum Ultra mass spectrometer (Thermo Scientific, West Palm Beach, FL) coupled with a Waters Acquity UPLC system (Waters, Milford, MA), as previously described (22). EVs isolated from equal numbers of cells treated with vehicle or PA were used to quantify changes in EV ceramides. Cell pellet ceramides were normalized to protein content. Ceramides in plasma EVs were measured in EVs isolated from equal volumes of plasma across experimental groups.

Electron microscopy

Whole mount preparations of isolated EVs were prepared for electron microscopy according to established methods (20). Briefly, EVs suspended in PBS were fixed with 2% paraformaldehyde, applied to Formvar carbon-coated EM grid, fixed with 1% glutaraldehyde, contrasted with uranyl-oxalate solution, embedded in a mixture of uranyl acetate and methylcellulose, air dried, and observed under the JEOL 1400 electron microscope (JEOL USA, Peabody, MA).

Western blotting

Treated cells were collected by scraping and lysed in RIPA buffer (50 mM Tris HCL, 1% NP-40, 0.1% SDS, 150 nM NaCl, 1 mM EDTA, and 0.5% sodium deoxycholate) with protease and phosphatase inhibitors. The protein concentrations were determined by the Bio-Rad DC protein assay (Bio-Rad, Hercules, CA). Equal amounts of protein were loaded onto Criterion 12.5% Tris-HCl gel (Bio-Rad) and electro-transferred to an Immobilion® -FL PVDF membrane (EMD Millipore). After washing, the membranes were incubated in 25 ml of blocking buffer (LI-COR Biosciences, Lincoln, NE) for 1 h at room temperature. Immunostaining was performed with the primary antibody [CD63, TSG101, and Sptlc-1 (Santa Cruz Biotechnologies); phospho-eIF2α (Invitrogen, Carlsbad, CA)], followed by incubation with IRDye 680RD and 800CW secondary antibodies (LI-COR). Immunoreactive proteins were detected with an infrared imaging system (LI-COR).

Immunofluorescence

Cells were cultured on cover slips in 6-well plates. After removing medium, cells were washed three times with PBS and fixed (0.1 M PIPES, 1.0 mM EGTA, 3.0 mM $MgSO_4$, and 2.5% formaldehyde). After washing with PBS, cells were permeabilized by Triton X-100. Blocking buffer (5% goat serum, 5% glycerol, and 0.04% sodium azide) was applied to fixed and permeabilized cells for 1 h followed by primary antibody overnight at 4°C. After washing with PBS, cells were incubated with secondary antibody for 1 h, washed with PBS, and mounted with 20 µl Prolong Anti-Fade (Life Technologies) on a clean glass slide. In the case of CD63 (Santa Cruz Biotechnologies), we used poly-L-lysine-coated cover slips (Sigma) for growing cells. Fluorescence was observed with confocal microscopy (LSM 780 Zeiss).

Quantitative real-time PCR

After assay medium was removed, cells were washed two times with PBS, collected in 1 ml Trizol, and the aqueous phase, after addition of 200 µl chloroform and centrifugation, was applied to the G-eliminator column (RNeasy Plus; Qiagen) and RNA was extracted from the flow-through according to the manufacturer's instructions. Quantity and quality of RNA was measured spectrophotometrically using a NanoDrop ND1000 (Thermo Scientific), and RNA was reverse transcribed into cDNA by the iScript cDNA synthesis kit (Bio-Rad). Quantitative real-time PCR reactions were run on the LightCycler 480 (Roche), using the LightCycler 480 SYBR Green 1 Master Mix (Roche) and previously published primers (16).

RNA interference

WT IMH cells were cultured in 6-well plates. The transient knockdown of SPT1 or X-box binding protein-1 (XBP-1) was performed using SPTLC1 siRNA (Santa Cruz Biotechnologies, sc-153804) or XBP-1 siRNA (Life Technologies, s76116), with control siRNA-A (Santa Cruz Biotechnologies, sc-37007) or Silencer Negative Control siRNA (Life Technologies) as negative controls. The siRNA transfection was performed using X-tremeGENE siRNA (Roche) for SPTLC1 or Lipofectamine RNAiMAX transfection reagent (Invitrogen) for XBP-1 according to manufacturer's instructions. S1P receptor 1 ($S1P_1$) was silenced in BMDMφs by electroporation, as described (23). Briefly, 2×10^6 cells were electroporated in a 4 mm cuvette (BTX Harvard Apparatus) with GenePulser Xcell (Bio-Rad) at 400 V, 150 µF, and 100 Ω. $S1P_1$ siRNA (L-05684-00-0005) and nontargeting siRNA (D-001810-10-05) were purchased from Dharmacon. After electroporation cells were grown on tissue culture plastic in serum-free RPMI for 30 min, an equal volume of bone marrow differentiation medium was added to achieve a final concentration of 10% FBS and 20% L929 conditioned medium. Seventy-two hours after electroporation cells were used for chemotaxis assays. Gene silencing was confirmed by Western blotting or reverse-transcription PCR.

Ceramide treatment

WT or IRE1α KO IMH cells were cultured to 90% confluency on 150 mm dishes and treated with C16 ceramide, as described (24). After washing with PBS, the medium was changed to assay medium supplemented with 10 µM C2 ceramide (Enzo, BML-SL100) or 10 µM C16 ceramide (Cayman, item number 10681), and then medium was recovered after 16 h for measuring EVs. Cells were cultured for 2–4 h under high-dose C16 ceramide (50 µM or 100 µM) conditions and the medium recovered for isolation of EVs.

CRISPR/Cas9 gene editing

The lentiCRISPRv1 and lentiCRISPRv2 plasmids were a gift from Dr. Feng Zhang and obtained from Addgene (25). The online tool (http://crispr.mit.edu) was used to design the single guide RNA spanning the first exon of human XBP-1 (sgRNA 5′-CACC-GGCGCTGTCGCTTGCGCGCC-3′), which is conserved between total and spliced XBP-1. Annealed oligonucleotides of sgRNA were used to generate a lentivirus following subcloning into the lentiCRISPRv1 plasmid (Addgene), and transfected into HEK 293T cells along with packaging plasmids, pCMV-VSV-G and pCMV-dR8.2 dvpr (Addgene), using Lipofectamine LTX reagent (Invitrogen). Virus was harvested 48 h after transfection and passed through at 0.45 µM pore cellulose acetate filter (Millipore). Huh7 cells were infected with XBP-1-targeting lentivirus in the presence of 8 µg/ml Polybrene. Successfully infected cells were selected under 2 µg/ml puromycin (Invitrogen) selection

pressure. XBP-1 KO was confirmed by Western blotting of nuclear extracts from cells treated with tunicamycin to induce ER stress.

Chemotaxis assays

Modified Boyden chambers (Neuro Probe, BW200S) were used to perform chemotaxis assays using 5 μm pore size polycarbonate track-etch membranes (Neuro Probe, PFA5), which were coated with 0.1% gelatin (Sigma, G1393) for 30 min and then air-dried. BMDMϕs were serum starved in 2% exosome-free FBS containing RPMI for 1 h and then pretreated with the appropriate treatment conditions for 1 h. Cells were detached in treatment conditions, counted, and diluted to a concentration of 250,000 cells/ml. Chambers were assembled with chemo-attractants on the bottom in 0.2 ml volume and pretreated cells were placed on top of the membrane in 0.2 ml volume. EVs isolated from equal numbers of vehicle- or PA-treated cells were used as chemo-attractants. PF543 (5 μM; Selleckchem) and ABC294640 (1 μM; Activebiochem) were employed to inhibit sphingosine kinase (SphK)1 and SphK2, respectively. W146 (1 μM; Cayman Chemical) or FTY720 (0.25 μM; Cayman Chemical) were used to antagonize S1P receptors. Cells were allowed to migrate for 4 h, fixed in 10% neutral buffered formalin for 20 min at room temperature, rinsed once in PBS and once in water, and mounted in Prolong Gold antifade reagent with DAPI (Life Technologies). Migrated cells were counted on a confocal microscope ((LSM 780 Zeiss) using a UV laser.

Mouse studies

All animal studies and use were approved by the institutional care and animal use committee of the Mayo Clinic and were conducted in accordance with the public health policy on the humane use and care of laboratory animals. Mice were housed in standard pathogen-free facilities with 12 h day-night circadian cycles and unrestricted access to food and water. C56Bl/6J mice were purchased from Jackson Laboratory (Bar Harbor, ME). Twelve-week-old mice were fed either chow or a diet high in saturated fat, fructose, and cholesterol (FFC) for 24 weeks, as previously described (26). This diet recapitulates the pathologic features of human NASH. Upon completion of the feeding study, blood was collected by cardiac puncture, and platelet-poor plasma was isolated by centrifugation at 1,200 g for 20 min at room temperature, followed by 13,000 g at 4°C for 2 min. Plasma was stored at −20°C until further analyses.

Human studies

This study was approved by the Institutional Review Board of the Mayo Clinic and all subjects provided written informed consent. Available archived liver samples from a previously published study were utilized (27). Subjects who had undergone liver biopsy during bariatric surgery for medically complicated obesity with body mass index of >30 kg/m^2 [at Mayo Clinic, Rochester, MN, with histologic categorization of the biopsies according to established NASH criteria by an experienced hepatopathologist into three groups] were included (28). The three groups were obese normal (normal liver biopsies, n = 4; plasma, n = 11), simple steatosis (liver biopsies, n = 4; plasma, n = 16), and NASH with early fibrosis (F0-1) (liver biopsies, n = 6; plasma, n = 16). Subjects with secondary causes of steatohepatitis and other chronic liver diseases were excluded [drugs, prior gastric surgery for obesity, excessive alcohol consumption, viral hepatitis (B, C), cholestatic liver disease, hemochromatosis, Wilson disease, drug-induced liver disease, and α-1-antitrypsin deficiency]. NAFLD activity score (NAS) was calculated as described, using the sum of steatosis, lobular inflammation, and hepatocyte ballooning

graded in a blinded manner by an experienced hepatopathologist (28). For lipidomic analyses, 20–25 mg frozen liver samples were powdered in liquid nitrogen, weighed, and homogenized in PBS to make a homogenate (10 μl/mg tissue). Fifty microliters of homogenates (5 mg of liver tissue) were used for sphingolipid and ceramide analysis.

Statistical and data analyses

Data represent mean ± SEM from three or more experiments unless indicated otherwise. Student's t-test and ANOVA were used for statistical analyses in GraphPad Prism version 6.00 for Windows (GraphPad Software, LaJolla, CA; www.graphpad.com). $P < 0.05$ was considered significant. JMP software (SAS Institute) was used for regression analyses.

RESULTS

PA induces the release of EVs

PA, a toxic saturated free fatty acid, induces hepatocellular apoptosis in a concentration- and time-dependent manner (4, 29). In order to measure cellular EV release prior to the onset of apoptosis, we established the concentration and duration for treating IMH and Huh7 cell lines with PA and Tg, a known inducer of ER stress signaling (15), such that there was no increase in cell death (supplementary Fig. 1A, B). Next, we measured EV release under these conditions. For each experimental condition, isolated EVs were normalized to cell number and expressed relative to the vehicle-treated condition. Following treatment of IMH cells with Tg or PA, a 2.9-fold increase in EV release in Tg-treated cells and a 7.7-fold increase in PA-treated cells were observed (**Fig. 1A**). We did not observe a significant EV response in cells treated with the nontoxic monounsaturated fatty acid, OA (Fig. 1A); therefore, we further analyzed Tg-induced and PA-induced EVs. EVs released under Tg or PA were similar in size to vehicle-treated cells, 117–124 nm (particle size, mode, Fig. 1B). Thus, the size distribution was not altered, although the magnitude of EVs released was significantly greater in cells treated with Tg or PA (Fig. 1C). We confirmed these findings in the human hepatoma cell line, Huh7 (Fig. 1D–F). Electron microscopy of IMH cells confirmed the characteristic morphology of EVs released under all three conditions (Fig. 1G). These particles expressed characteristic extracellular microparticle markers, Tsg101 and CD63 (Fig. 1H) (10). Furthermore, when cultured on poly-L-lysine-coated coverslips, thereby increasing adhesion between EVs and the coverslip, we could detect extracellular CD63-expressing particles (supplementary Fig. 1C). A significant increase in PA-induced EV release was also observed in primary mouse hepatocytes (**Fig. 2A**). All together, these data demonstrate a significant increase in EV release from mouse and human hepatocyte cell lines and primary mouse hepatocytes treated with either Tg or PA. The consistency of the response between Tg and PA suggested that an ER stress sensor was promoting the stress-induced EV release.
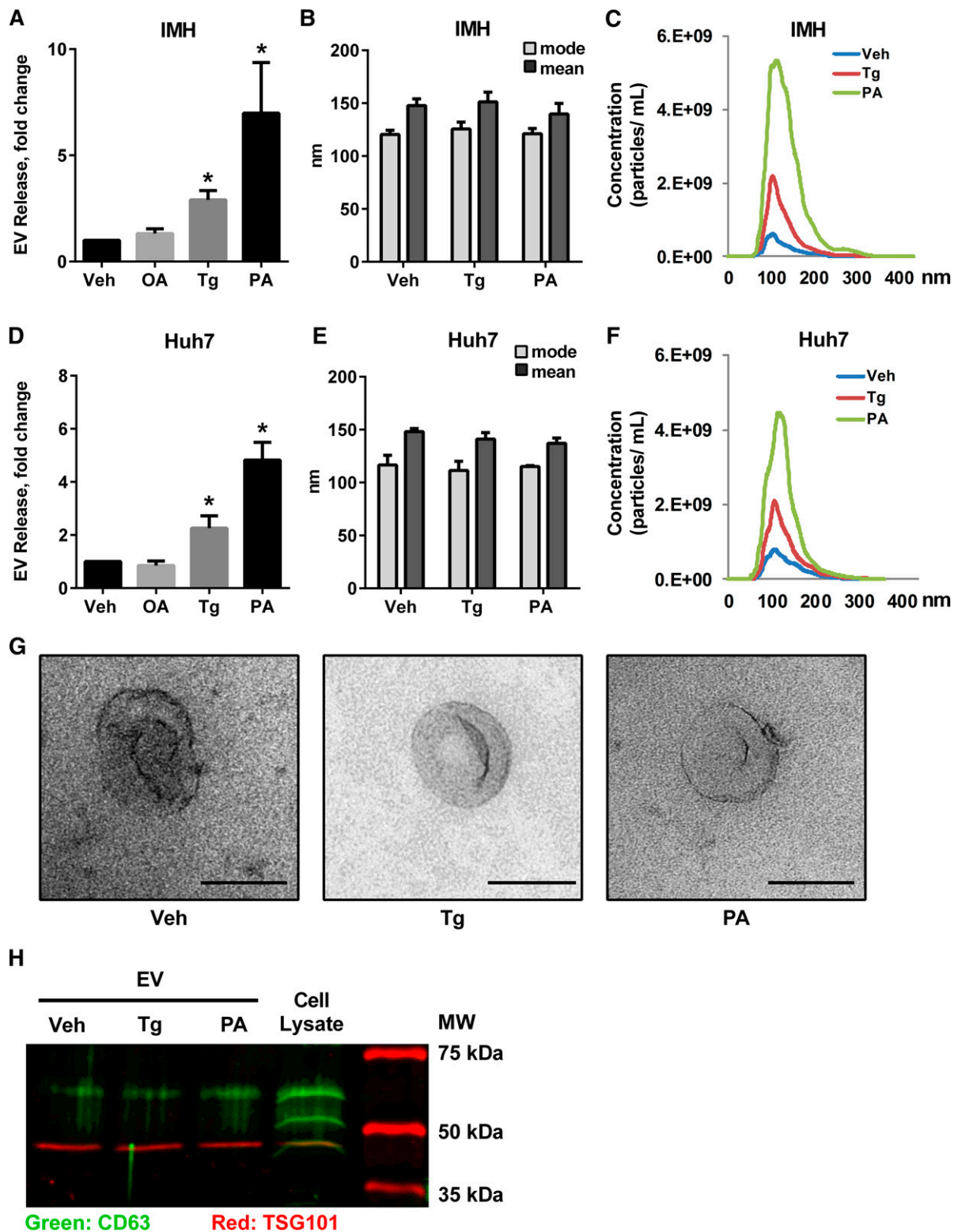
Fig. 1. PA induces EV release from hepatocytes. IMHs or human hepatoma cells (Huh7) were treated with 2.5 nM Tg, 400 μM OA, 400 μM PA, or vehicle (Veh) for 16 h. Fold increase in EV release (A, D), size distribution (B, E), and concentration and size distribution (C, F) are depicted. G: Morphology of representative EVs by electron microscopy from IMH cells treated as indicated; scale bar equals 100 nm. H: EV makers were confirmed by Western blotting for CD63 and Tsg101. The rightmost lane indicates molecular mass. *$P < 0.05$ compared with vehicle-treated cells.

IRE1α mediates the release of EVs

We confirmed activation of IRE1α signaling via the splicing of XBP-1 and activation of PERK signaling via phosphorylation of eIF2α and transcriptional upregulation of CHOP in hepatocytes treated with PA (supplementary Fig. 2A–C). To ascertain which of the three ER stress
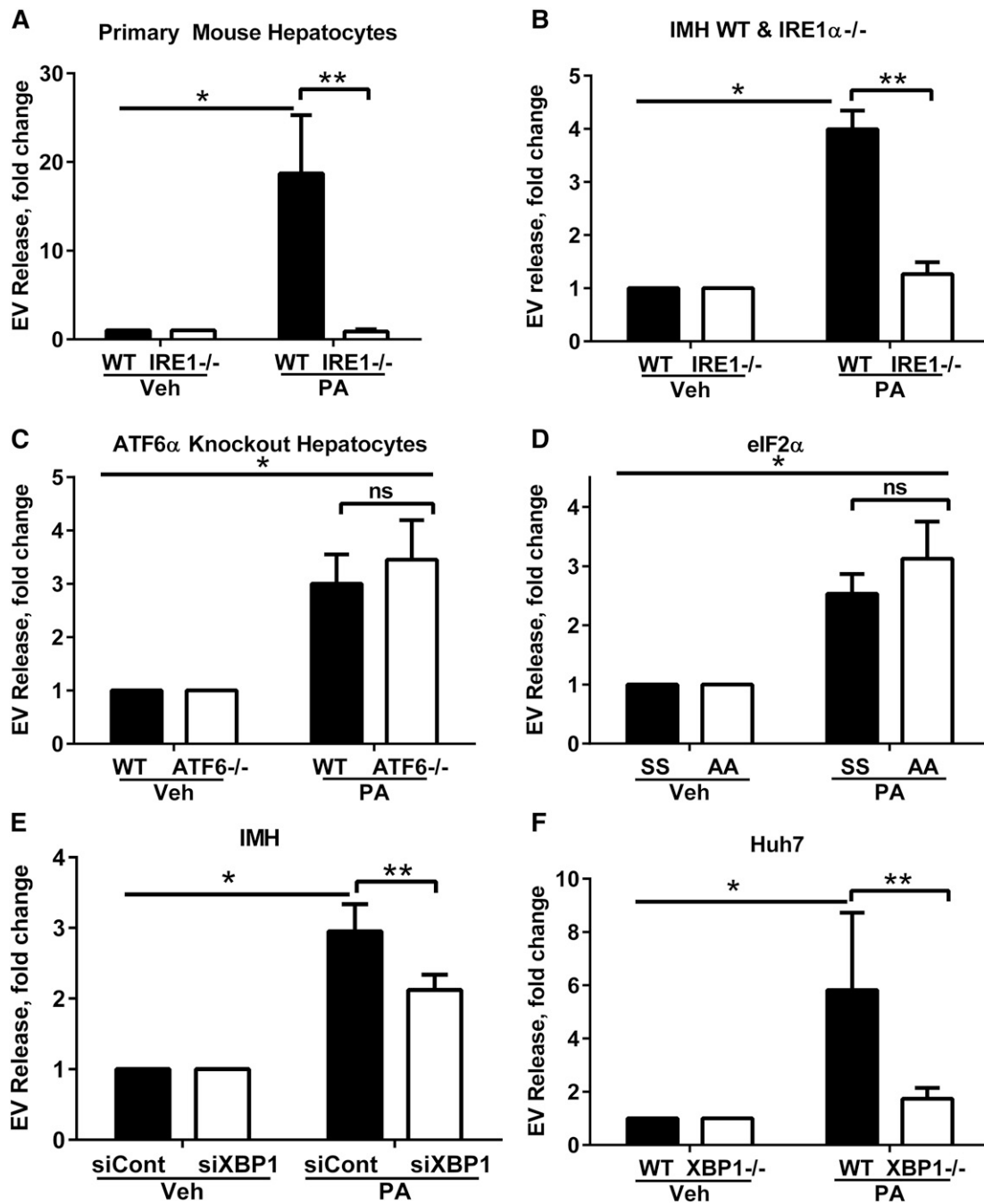
Fig. 2. EV release is IRE1α/XBP-1 dependent. A: EV response in primary mouse hepatocytes from WT and IRE1α hepatocyte-specific KO mice treated with 200 μM PA for 14 h. B: IMH from WT and IRE1α hepatocyte-specific KO mice (IRE1$^{-/-}$) treated with 400 μM PA for 16 h. *$P < 0.05$ for PA-treated WT cells compared with vehicle (Veh). **$P < 0.05$ for PA-treated WT cells compared with KO. EV response in ATF6α WT and KO cells (C) and eIF2α phosphorylation resistant (AA) and WT (SS) cells treated with 400 μM PA or vehicle for 16 h (D). *$P < 0.05$ for PA-treated cells compared with vehicle. E: XBP-1 was knocked down in IMH cells using siRNA (siXBP1) and a nontargeting siRNA was used as a control (siCont). EVs were isolated using a commercially available polymer-based reagent. *$P < 0.05$ for PA-treated si-Cont cells compared with vehicle. **$P < 0.05$ for PA-treated siCont cells compared with siXBP1. F: EVs from XBP-1 deleted Huh7 (XBP1$^{-/-}$) cells using the CRISPR/Cas9 genome editing technology, treated with 400 μM PA or vehicle for 16 h, were isolated using a commercially available polymer-based reagent. *$P < 0.05$ for PA-treated WT cells compared with vehicle. **$P < 0.05$ for PA-treated WT cells compared with XBP1$^{-/-}$.

sensors might be contributing to the enhanced EV release, we employed a series of genetically deficient cell lines. Furthermore, as Tg is not a pathophysiologically relevant ER stress-inducing agent and due to the pathophysiologic importance of PA-induced lipotoxicity in the pathogenesis of NASH, we focused our subsequent experiments on PA,

due to its obvious disease relevance. Initially, we isolated primary mouse hepatocytes from WT and IRE1α hepato-cyte-specific KO mice, treated them with PA, and measured the EV response. The PA-induced EV response was significantly reduced in IRE1α-KO hepatocytes (Fig. 2A). The IRE1α-dependent release of PA-induced EV release

was further tested in the IMH cell lines. Consistent with the data from the primary mouse hepatocytes, the deletion of IRE1α led to a significant reduction in the PA-induced EV response (Fig. 2B). To determine whether this phenomenon was a consequence of the general unfolded protein response or specific to IRE1α, we treated cell lines genetically deleted in ATF6α or cell lines mutated at serine 51 (to alanine), rendering a phosphorylation-resistant eIF2α (thus inactive) with PA (30, 31). Both, ATF6α WT and KO cells had an equivalent EV response to PA (Fig. 2C). Similarly, interrogation of the PERK signaling pathway was accomplished by employing eIF2α WT and phosphorylation-resistant cell lines, both of which had comparable induction of an EV response to PA (Fig. 2D). Thus, these experiments confirmed that PA-induced EV release specifically involves the IRE1α branch of the ER stress response.

EV release requires the canonical IRE1α target, XBP-1

IRE1α activates its canonical target, XBP-1, a potent transcription factor that mediates its signaling function (15). Thus, we next examined the need for XBP-1 signaling in the IRE1α dependence of PA-induced EV release. We approached this by generating XBP-1 deleted cell lines using RNA interference or the CRISPR/Cas9 genome editing technology (25). In IMH cells with XBP-1 knockdown using siRNA, we observed an attenuation of PA-induced EV release (Fig. 2E). Next, the human Huh7 cells were deleted in XBP-1 ($XBP1^{-/-}$) and treated with PA. The PA-induced EV release was significantly reduced in the $XBP1^{-/-}$ Huh7 cell line (Fig. 2F). All together, these studies suggest that XBP-1 mediates PA-induced EV release following IRE1α activation.

EVs are enriched in C16:0 ceramide

Given the role for ceramides in EV generation, we next measured EV ceramide and sphingolipid content by tandem mass spectrometry (**Fig. 3A**). There was a significant enrichment in C16:0 ceramide in IRE1α WT IMHs treated with PA (Fig. 3A). Consistent with a lack of EV response in cells lacking IRE1α, an increase in EV C16:0 ceramide was not observed in IRE1α KO IMHs. An increase in whole cell C16:0 ceramide in PA-treated IRE1α WT IMH cells was also observed, with lack of an increase in IRE1α KO cells (Fig. 3B). The formation of 3-ketosphinganine from PA and serine, the rate-limiting step in de novo ceramide synthesis, is catalyzed by serine palmitoyltransferase (SPT) (32). Therefore, we hypothesized that inhibition of this enzyme would mitigate an EV response. Cells treated with myriocin, a pharmacologic inhibitor of SPT, displayed reduced PA-mediated EV release (Fig. 3C). Conversely, we treated cells with C16:0 ceramide to determine whether exogenous loading of C16:0 ceramide would lead to EV release. We predicted that C16:0 ceramide loading would restore an EV release response in IRE1α KO cells by bypassing the need for ceramide biosynthesis. Indeed, in both WT and IRE1α KO cells, C16:0 ceramide treatment led to a significant increase in EV release (Fig. 3D). The response to C16:0 ceramide was concentration dependent

in both IRE1α WT and KO cells (Fig. 3E). Lastly, treating cells with a short chain C2 ceramide did not lead to an EV response, demonstrating specificity for physiologically relevant ceramides in this process (Fig. 3F). Thus, IRE1α-dependent accumulation of C16:0 ceramide leads to the release of C16:0 ceramide-enriched EVs in PA-treated hepatocytes.

IRE1α regulates SPT1

To elucidate the mechanism by which PA induces an IRE1α-dependent EV response, we examined the regulation of SPT1. SPT1 is one of the three subunits that are required for the formation of the functional heterodimeric enzyme. SPT1 mRNA expression was induced by PA treatment in IRE1α WT cells. This induction of SPT1 mRNA did not occur in IRE1α KO cells (Fig. 3G). To determine whether SPT1 mediated PA-induced EV release, we used a siRNA approach; validation of the SPT1 knockdown was confirmed by immunoblot analysis (Fig. 3H). There was a significant reduction in PA-induced EV release in cells deficient in SPT1 (Fig. 3H). As anticipated, exogenous application of C16:0 ceramide to cells silenced in SPT1 led to a restoration of EV secretion (Fig. 3H), similar to the data in IRE1α KO cells. Thus, PA-induced ceramide biosynthesis occurs via IRE1α induction of SPT1 expression.

PA-induced EVs are chemotactic to macrophages

To determine a biologic role for lipotoxic EVs, we focused on macrophage chemotaxis, as macrophages recruited to the liver are known to be pro-inflammatory in NASH (17). We treated primary BMDMφs with EVs derived from PA-treated or vehicle-treated cells. PA-derived EVs induced significant chemotaxis in BMDMφs (**Fig. 4A**). To elucidate a mechanism for lipotoxic C16:0 ceramide-enriched EV-induced macrophage chemotaxis, we asked whether S1P signaling might mediate macrophage migration. S1P is formed by the phosphorylation of C16:0 ceramide-derived sphingosine by SphK1 and SphK2 (33). Newly formed S1P is released by cells into the extracellular milieu where it binds cell membrane receptors and stimulates downstream signaling, the classical inside-out autocrine signaling (33). Therefore, we reasoned that if ceramide transfer to macrophages was providing a substrate for S1P generation, inhibitors of both SphKs and S1P receptors (S1PRs) would inhibit macrophage migration. We first used pharmacologic inhibitors of SphK1 and SphK2. Both inhibitors significantly inhibited macrophage migration toward PA-stimulated lipotoxic EVs (Fig. 4B), suggesting that the synthesis of S1P by macrophages was necessary for lipotoxic EV-induced macrophage migration. Next, we used S1PR inhibitors to assess their effect on macrophage migration. We employed FTY720, which binds S1P receptors 1, 3, 4, and 5 (though functionally antagonizing $S1P_1$), and W146, a specific antagonist of $S1P_1$ receptor (34). Both inhibitors significantly reduced PA-stimulated EV-induced migration of both Raw264.7 cells (Fig. 4C) and BMDMφs (Fig. 4D). Next, to confirm that $S1P_1$ mediated macrophage migration, we employed RNA silencing. BMDMφs deficient in $S1P_1$ demonstrated a
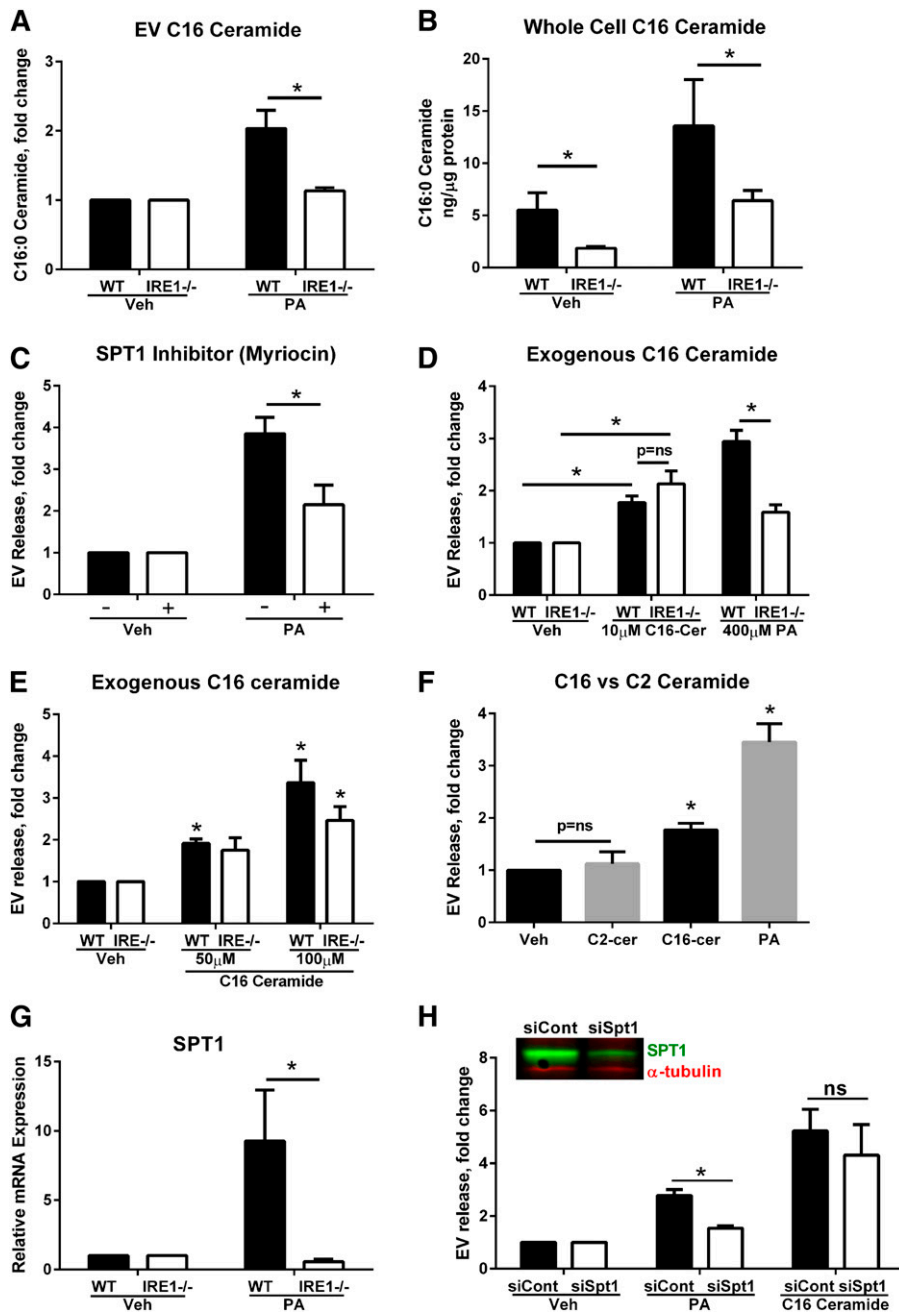
Fig. 3. C16 ceramide synthesis is necessary for IRE1α-dependent PA-induced EV release. A: EVs isolated from WT or IRE1α KO (IRE1$^{-/-}$) IMHs were treated with 400 μM PA or vehicle (Veh). The C16 ceramide content of EVs was measured by LC-MS/MS. EVs isolated from three independent experiments were pooled for lipidomics analysis. B: C16 ceramide was measured in whole cell pellets, under the same conditions as (A), and normalized to protein content. *$P < 0.05$ for the comparisons shown. C: EVs were isolated from IMHs treated with PA or vehicle, with or without 10 μM myriocin. *$P < 0.05$ for the comparisons shown. D: EVs isolated from WT or IRE1α KO (IRE1$^{-/-}$) IMHs treated with 10 μM exogenous C16:0 ceramide (C16-Cer) or PA for 16 h. *$P < 0.05$ for the comparisons shown. E: EVs isolated from WT or IRE1α KO (IRE1$^{-/-}$) IMHs treated with 50 and 100 μM exogenous C16:0 ceramide for 4 h. *$P < 0.05$ compared with vehicle-treated cells. F: EVs were isolated from IMHs treated with 10 μM exogenous C16 ceramide, 10 μM C2 ceramide, or 400 μM PA for 16 h. *$P < 0.05$ compared with vehicle-treated cells. G: WT or IRE1α KO (IRE1$^{-/-}$) IMHs were treated with 400 μM PA or vehicle (Veh) for 4 h, and the expression of SPT1 mRNA was measured. *$P < 0.05$ for PA treated cells. H: IMHs were transfected with SPT1 siRNA or a control siRNA for 72 h. The efficiency of silencing was analyzed by SPT1 Western blotting (inset). EVs were isolated from PA- or vehicle-treated cells using a commercially available polymer, and from C16 ceramide-treated cells (100 μM, 4 h) with ultracentrifugation. *$P < 0.05$ for PA-treated cells; ns, not significant.
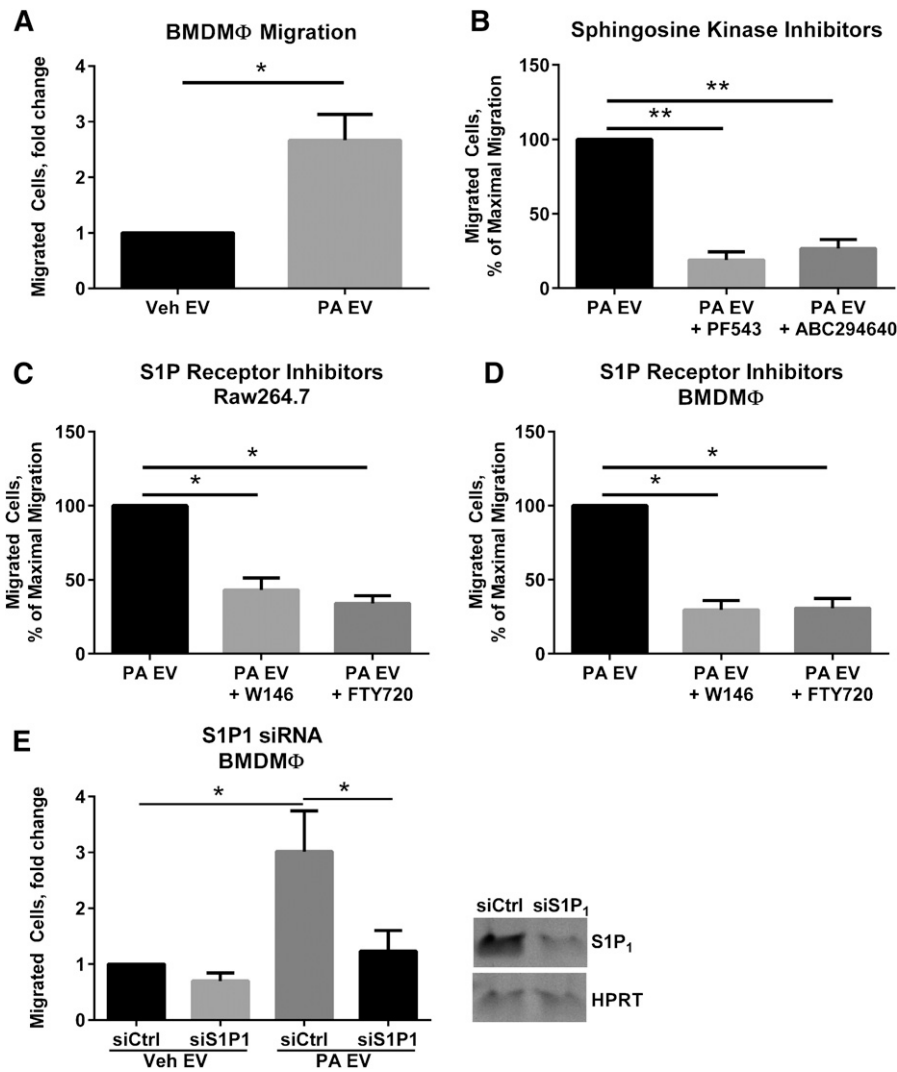
Fig. 4. Lipotoxic EVs activate S1P receptor-mediated macrophage migration. A: Mouse BMDMφs were migrated for 4 h toward EVs derived from equal numbers of cells treated with 400 μM PA or vehicle (Veh) for 16 h. B: BMDMφs were pretreated with 5 μM PF543 or 1 μM ABC294640 for 1 h before migration toward lipotoxic EVs was assessed. C: Mouse macrophage cell line Raw246.7 (C) or BMDMφs (D) were pretreated with 0.25 μM FTY720 or 1 μM W146 for 1 h before migration toward lipotoxic EVs was assessed. E: siRNA targeting $S1P_1$ or control nontargeting siRNA were delivered to BMDMφs, which were subsequently migrated for 4 h toward EVs derived from equal numbers of cells treated with 400 μM PA or vehicle for 16 h. The inverted gel image shows $S1P_1$ expression in BMDMφs treated with nontargeting siRNA (siCtrl) or $S1P_1$ (siS1P₁). *$P < 0.05$ and ** $P < 0.001$ for the comparisons shown.

significant attenuation in lipotoxic EV-induced migration (Fig. 4E). These data suggest a potential pro-inflammatory role for PA-induced EVs by promoting macrophage recruitment to the liver via $S1P_1$ receptor-mediated macrophage chemotaxis.

Ceramides are enriched in circulating EVs derived from murine and human NASH

Having demonstrated an EV response under PA-induced lipotoxic conditions with a concomitant ER stress response, we next asked whether circulating EVs were increased in a diet-induced model of murine NASH. Mice were fed either chow or a diet high in FFC for 24 weeks. Circulating EVs were significantly increased in FFC-fed mice (**Fig. 5A**). We measured the C16:0 ceramide and S1P

content of circulating EVs from both chow-fed and FFC-fed mice. C16:0 ceramide was significantly enriched in mouse plasma EVs in FFC-fed mice (Fig. 5B). Corresponding liver samples demonstrated a significant increase in C16:0 ceramide in FFC-fed livers (Fig. 5D). Though the S1P content was increased in FFC-fed circulating EVs and mouse liver samples, this did not reach statistical significance (Fig. 5C, E). To expand our observations on the ceramide and S1P content of circulating mouse EVs in NASH to human subjects, we analyzed plasma EVs from obese normal, simple steatosis, and NASH with early fibrosis. Macrophage recruitment to the liver is an early event in NASH pathogenesis, and as we are interested in understanding these early "liver homing" signals in disease pathogenesis, we included only NASH with early fibrosis
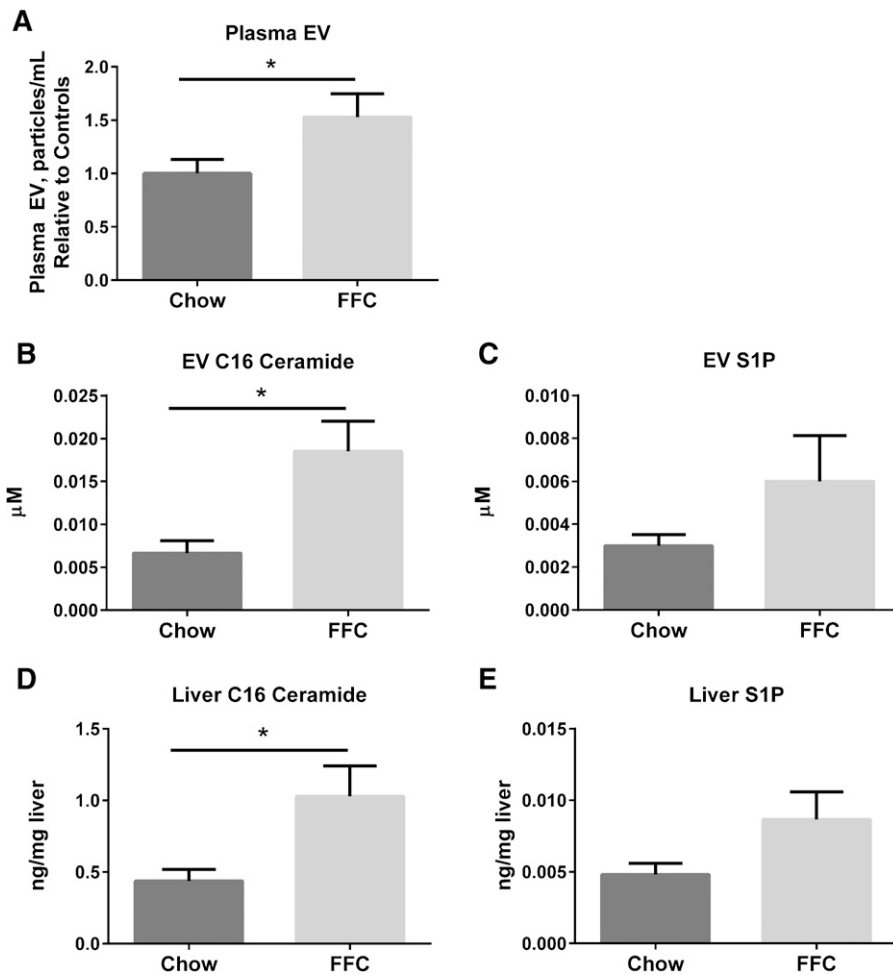
Fig. 5. C16:0 ceramide and S1P in murine NASH. A: Circulating EVs were measured in 100 µl of plasma from mice fed either chow (n = 9) or the FFC NASH-inducing diet (n = 10) for 24 weeks. C16:0 ceramide (B) and S1P (C) were measured in EVs isolated from 100 µl of plasma from the mice described in (A). C16:0 ceramide (D) and S1P (E) were measured in liver samples from the mice described in (A). *$P < 0.05$ for the comparisons shown.

subjects in this analysis. The NAS was significantly higher in subjects with NASH compared with simple steatosis (**Fig. 6A**); obese normal subjects has normal liver histology. Consistent with the mouse findings, circulating EVs were significantly elevated in human NASH, and were significantly enriched in C16:0 ceramide and S1P (Fig. 6B–D). Interestingly, plasma C16:0 ceramide and S1P exhibited a reciprocal relationship (Fig. 6E, F; supplementary Fig. 3) with EV C16:0 ceramide and S1P, such that in NASH subjects there was depletion in circulating plasma levels of these bio-active lipids, though an increase in their enrichment in EVs. Thus, there may be a selective partitioning of hepatocyte-derived sphingolipids into EVs in NASH. These findings would need substantiation in larger cohorts. Furthermore, we found an increase in C16:0 ceramide and not S1P in corresponding liver biopsy samples (Fig. 6G, H).

DISCUSSION

In this study, we have elucidated a mechanistic basis for the release of pro-inflammatory EVs under hepatic lipotoxic conditions. The principal findings of this study are: *i*) PA-treated hepatocytes release EVs in an IRE1α-dependent manner; *ii*) lipotoxic EVs are enriched in C16:0 ceramide, and IRE1α-regulated de novo ceramide biosynthesis is necessary for PA-stimulated EV release; *iii*) lipotoxic EVs stimulate macrophage chemotaxis via S1P generation; and *iv*) ceramide-enriched circulating EVs are increased in mouse and human NASH. These data provide a mechanistic link between lipotoxic ER stress and disease pathogenesis, suggesting that the observed IRE1α activation in NASH livers may promote secretion of C16:0 ceramide-enriched EVs from steatotic hepatocytes, thus likely promoting macrophage recruitment to the liver.

PA induces ER stress and activates all three of the unfolded protein response sensors (16, 35). We have extended these observations by demonstrating that PA-mediated ER stress stimulates EV release from hepatocytes. The PA-stimulated EV release was specific for the ER stress sensor, IRE1α. In cells lacking ATF6α or cells resistant to PERK-induced eIF2α phosphorylation due to a phosphorylation resistant mutation at serine 51 of eIF2α, the PA-induced EV response was intact. Next, we defined
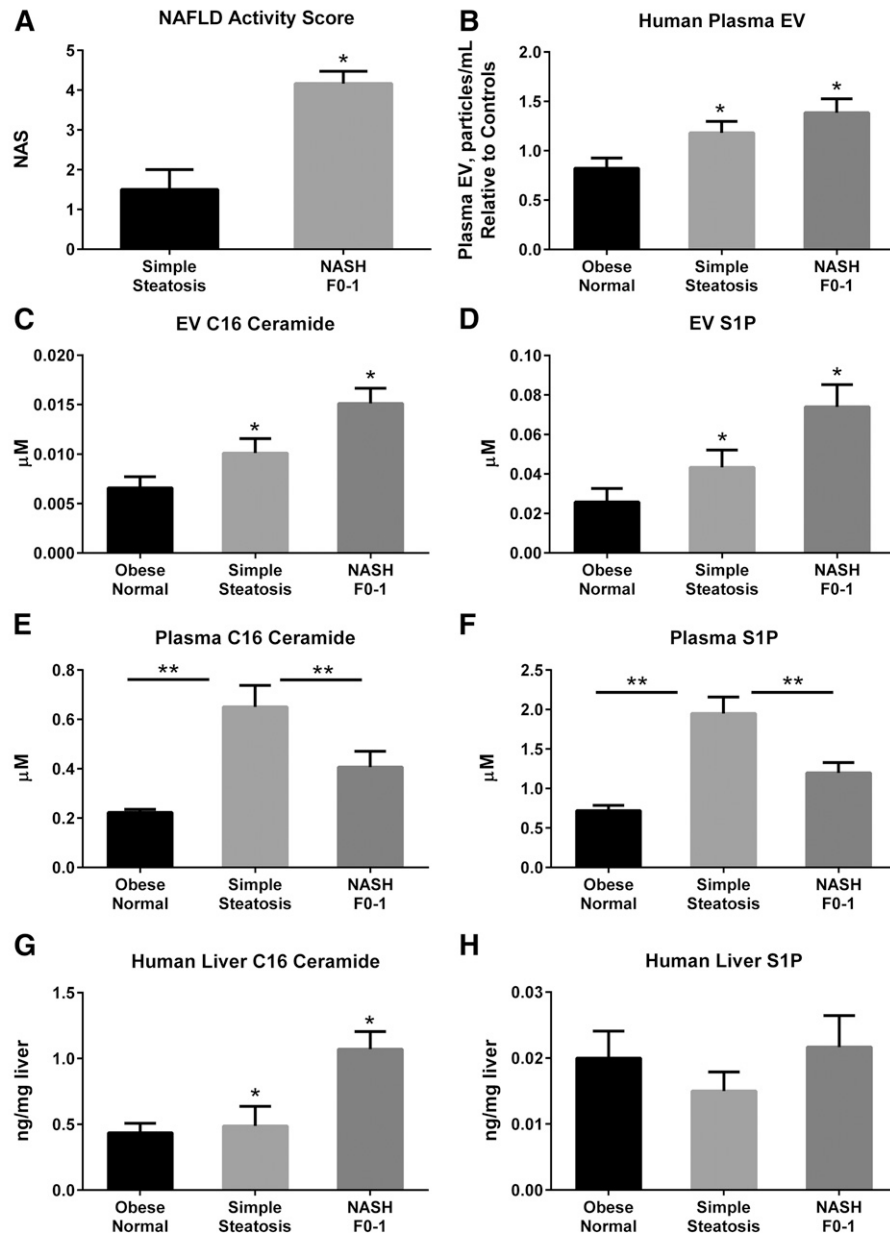
Fig. 6. C16:0 ceramide and S1P in human NASH. A: NAS for subjects with simple steatosis (n = 4) and early NASH F0-1 (n = 6). B: Circulating EVs were measured in 900 μl of plasma obtained from obese normal (n = 11), simple steatosis (n = 16), and early NASH F0-1 (n = 16). Particle concentration is expressed relative to the averaged obese normal. C16:0 ceramide (C) and S1P (D) were measured in EVs isolated from 900 μl of plasma from the subjects described in (B). C16:0 ceramide (E) and S1P (F) were measured in 25 μl of plasma samples from the subjects described in (A), in whom matching liver biopsy samples were available: obese normal (n = 4), simple steatosis (n = 4), and early NASH F0-1 (n = 6). C16:0 ceramide (G) and S1P (H) were measured in available liver biopsy samples from the subjects described in (E). *$P < 0.05$ by ANOVA for comparisons involving all three groups; **$P < 0.05$ for the comparisons shown across two experimental conditions.

the mechanism for this observation by demonstrating that XBP-1 mediates this EV response by transcriptionally up-regulating its target, SPT, the rate-limiting enzyme of de novo ceramide biosynthesis (33).

As endosomes mature from early to late, thus forming MVBs, they interact intimately with the ER and ceramides synthesized in the ER are rapidly transported and transferred to the Golgi complex and eventually to the plasma membrane; thus, either or both of these cellular trafficking pathways could contribute to the formation and release of PA-induced vesicles. Furthermore, ceramide generation via acid and neutral sphingomyelinases is known to mediate vesicle release, especially vesicles derived from the MVB (14, 36), and play a role in the sorting of proteo-lipid cargo to vesicles. To our knowledge, this is the first demonstration that de novo ceramide biosynthesis via SPT is necessary for the biogenesis of EVs. Whether these EVs are derived from membrane shedding or from

MVB fusion to the plasma membrane is a question we will address in future studies.

EVs shed from cells can serve many roles, including the activation of target cells via the cargo they carry. They can activate target cells such as macrophages (37), enhance angiogenesis (11), promote tumor metastases (37), and transfer transcriptionally competent and regulatory RNA molecules to recipient cells (10). Herein, we demonstrate a chemotactic role for PA-induced EVs in our in vitro system. Our data implicate the activation of the $S1P_1$ receptor on macrophages by ceramide-derived S1P on lipotoxic EVs as the chemotactic stimulus. Though pharmacologic inhibitors can be nonspecific, FTY720 is known to functionally antagonize $S1P_1$, and W146 is highly selective for $S1P_1$ at the concentrations used (34). Additionally, using RNA interference, we show that macrophage migration is mediated, in part, by $S1P_1$, though other receptors may contribute. The S1P and SIP_1 signaling axis has been implicated in lymphocyte trafficking in sterile inflammatory conditions (33); here we advance this observation to potentially mediating macrophage recruitment to the steatotic liver.

Our findings of plasma EV and hepatic S1P and C16:0 ceramide enrichment in both mouse and human NASH are an essential biologic correlate to our in vitro findings. Recent mouse studies have demonstrated a critical pathogenic role for hepatic C16:0 ceramide in the pathogenesis of diet-induced obesity-related fatty liver. Our data might provide a mechanism by which C16:0 ceramide and its derivative, S1P, are pro-inflammatory by leading to the recruitment of myeloid cells to the liver, and potentially to other target organs. We acknowledge that a limitation of our human study is its small size. However, others also have independently demonstrated increased hepatic ceramides in models of NAFLD (38). Interestingly, we noted an increase in C16:0 ceramide and S1P in EVs from subjects with early NASH compared with simple steatosis and obese normal livers, suggesting that these may be an early liver-homing signal, attracting macrophages to the steatotic liver. It is also possible that EVs shed under these conditions perpetuate, rather than initiate, liver inflammation.

EVs are an emerging biomarker (10). They have been investigated in numerous human diseases and in mouse models of disease (10), and an increase in circulating EVs is described in a mouse model of NASH (39). Our findings further these observations, and suggest that the ceramide and S1P content of EVs might serve as an additional bio-active biomarker in NASH patients.

In conclusion, this is the first report linking PA-induced IRE1α activation to the release of pro-inflammatory EVs by lipotoxic hepatocytes. Our data suggest a mechanism for myeloid cell recruitment to the liver and the use of EVs as a bio-active biomarker. Additionally, several potential pathways for therapeutic intervention are identified, e.g., interference with the S1P signaling axis in macrophages.

REFERENCES

1. Rinella, M. E. 2015. Nonalcoholic fatty liver disease: a systematic review. *JAMA.* **313:** 2263–2273.
2. Lassailly, G., R. Caiazzo, D. Buob, M. Pigeyre, H. Verkindt, J. Labreuche, V. Raverdy, E. Leteurtre, S. Dharancy, A. Louvet, et al. 2015. Bariatric surgery reduces features of nonalcoholic steatohepatitis in morbidly obese patients. *Gastroenterology.* **149:** 379–388.
3. Nehra, V., P. Angulo, A. L. Buchman, and K. D. Lindor. 2001. Nutritional and metabolic considerations in the etiology of nonalcoholic steatohepatitis. *Dig. Dis. Sci.* **46:** 2347–2352.
4. Malhi, H., S. F. Bronk, N. W. Werneburg, and G. J. Gores. 2006. Free fatty acids induce JNK-dependent hepatocyte lipoapoptosis. *J. Biol. Chem.* **281:** 12093–12101.
5. Kakisaka, K., S. C. Cazanave, C. D. Fingas, M. E. Guicciardi, S. F. Bronk, N. W. Werneburg, J. L. Mott, and G. J. Gores. 2012. Mechanisms of lysophosphatidylcholine-induced hepatocyte lipoapoptosis. *Am. J. Physiol. Gastrointest. Liver Physiol.* **302:** G77–G84.
6. Holland, W. L., J. T. Brozinick, L. P. Wang, E. D. Hawkins, K. M. Sargent, Y. Liu, K. Narra, K. L. Hoehn, T. A. Knotts, A. Siesky, et al. 2007. Inhibition of ceramide synthesis ameliorates glucocorticoid-, saturated-fat-, and obesity-induced insulin resistance. *Cell Metab.* **5:** 167–179.
7. Park, T. S., W. Rosebury, E. K. Kindt, M. C. Kowala, and R. L. Panek. 2008. Serine palmitoyltransferase inhibitor myriocin induces the regression of atherosclerotic plaques in hyperlipidemic ApoE-deficient mice. *Pharmacol. Res.* **58:** 45–51.
8. Turpin, S. M., H. T. Nicholls, D. M. Willmes, A. Mourier, S. Brodesser, C. M. Wunderlich, J. Mauer, E. Xu, P. Hammerschmidt, H. S. Bronneke, et al. 2014. Obesity-induced CerS6-dependent C16:0 ceramide production promotes weight gain and glucose intolerance. *Cell Metab.* **20:** 678–686.
9. Raichur, S., S. T. Wang, P. W. Chan, Y. Li, J. Ching, B. Chaurasia, S. Dogra, M. K. Ohman, K. Takeda, S. Sugii, et al. 2014. CerS2 haploinsufficiency inhibits beta-oxidation and confers susceptibility to diet-induced steatohepatitis and insulin resistance. *Cell Metab.* **20:** 687–695. [Erratum. 2014. *Cell Metab.* **20:** 919.]
10. Raposo, G., and W. Stoorvogel. 2013. Extracellular vesicles: exosomes, microvesicles, and friends. *J. Cell Biol.* **200:** 373–383.
11. Povero, D., A. Eguchi, I. R. Niesman, N. Andronikou, X. de Mollerat du Jeu, A. Mulya, M. Berk, M. Lazic, S. Thapaliya, M. Parola, et al. 2013. Lipid-induced toxicity stimulates hepatocytes to release angiogenic microparticles that require Vanin-1 for uptake by endothelial cells. *Sci. Signal.* **6:** ra88.
12. Kornek, M., M. Lynch, S. H. Mehta, M. Lai, M. Exley, N. H. Afdhal, and D. Schuppan. 2012. Circulating microparticles as disease-specific biomarkers of severity of inflammation in patients with hepatitis C or nonalcoholic steatohepatitis. *Gastroenterology.* **143:** 448–458.
13. Nojima, H., C. M. Freeman, R. M. Schuster, L. Japtok, B. Kleuser, M. J. Edwards, E. Gulbins, and A. B. Lentsch. Hepatocyte exosomes mediate liver repair and regeneration via sphingosine-1-phosphate. *J. Hepatol.* Epub ahead of print. August 5, 2015; doi:10.1016/j.jhep.2015.07.030.
14. Trajkovic, K., C. Hsu, S. Chiantia, L. Rajendran, D. Wenzel, F. Wieland, P. Schwille, B. Brugger, and M. Simons. 2008. Ceramide triggers budding of exosome vesicles into multivesicular endosomes. *Science.* **319:** 1244–1247.
15. Malhi, H., and R. J. Kaufman. 2011. Endoplasmic reticulum stress in liver disease. *J. Hepatol.* **54:** 795–809.
16. Malhi, H., E. M. Kropp, V. F. Clavo, C. R. Kobrossi, J. Han, A. S. Mauer, J. Yong, and R. J. Kaufman. 2013. C/EBP homologous protein-induced macrophage apoptosis protects mice from steatohepatitis. *J. Biol. Chem.* **288:** 18624–18642.
17. Morinaga, H., R. Mayoral, J. Heinrichsdorff, O. Osborn, N. Franck, N. Hah, E. Walenta, G. Bandyopadhyay, A. R. Pessentheiner, T. J. Chi, et al. 2015. Characterization of distinct subpopulations of hepatic macrophages in HFD/obese mice. *Diabetes.* **64:** 1120–1130.
18. Zhang, K., S. Wang, J. Malhotra, J. R. Hassler, S. H. Back, G. Wang, L. Chang, W. Xu, H. Miao, R. Leonardi, et al. 2011. The unfolded

protein response transducer IRE1alpha prevents ER stress-induced hepatic steatosis. *EMBO J.* **30:** 1357–1375.

19. Faubion, W. A., M. E. Guicciardi, H. Miyoshi, S. F. Bronk, P. J. Roberts, P. A. Svingen, S. H. Kaufmann, and G. J. Gores. 1999. Toxic bile salts induce rodent hepatocyte apoptosis via direct activation of Fas. *J. Clin. Invest.* **103:** 137–145.

20. Thery, C., S. Amigorena, G. Raposo, and A. Clayton. 2006. Isolation and characterization of exosomes from cell culture supernatants and biological fluids. *Curr. Protoc. Cell Biol.* **Chapter 3:** 3.22.

21. van der Pol, E., F. A. Coumans, A. E. Grootemaat, C. Gardiner, I. L. Sargent, P. Harrison, A. Sturk, T. G. van Leeuwen, and R. Nieuwland. 2014. Particle size distribution of exosomes and microvesicles determined by transmission electron microscopy, flow cytometry, nanoparticle tracking analysis, and resistive pulse sensing. *J. Thromb. Haemost.* **12:** 1182–1192.

22. Blachnio-Zabielska, A. U., X. M. Persson, C. Koutsari, P. Zabielski, and M. D. Jensen. 2012. A liquid chromatography/tandem mass spectrometry method for measuring the in vivo incorporation of plasma free fatty acids into intramyocellular ceramides in humans. *Rapid Commun. Mass Spectrom.* **26:** 1134–1140.

23. Wiese, M., K. Castiglione, M. Hensel, U. Schleicher, C. Bogdan, and J. Jantsch. 2010. Small interfering RNA (siRNA) delivery into murine bone marrow-derived macrophages by electroporation. *J. Immunol. Methods.* **353:** 102–110.

24. Rénert, A. F., P. Leprince, M. Dieu, J. Renaut, M. Raes, V. Bours, J. P. Chapelle, J. Piette, M. P. Merville, and M. Fillet. 2009. The proapoptotic C16-ceramide-dependent pathway requires the death-promoting factor Btf in colon adenocarcinoma cells. *J. Proteome Res.* **8:** 4810–4822.

25. Sanjana, N. E., O. Shalem, and F. Zhang. 2014. Improved vectors and genome-wide libraries for CRISPR screening. *Nat. Methods.* **11:** 783–784.

26. Charlton, M., A. Krishnan, K. Viker, S. Sanderson, S. Cazanave, A. McConico, H. Masuoko, and G. Gores. 2011. Fast food diet mouse: novel small animal model of NASH with ballooning, progressive fibrosis, and high physiological fidelity to the human condition. *Am. J. Physiol. Gastrointest. Liver Physiol.* **301:** G825–G834.

27. Cazanave, S. C., J. L. Mott, N. A. Elmi, S. F. Bronk, N. W. Werneburg, Y. Akazawa, A. Kahraman, S. P. Garrison, G. P. Zambetti, M. R. Charlton, et al. 2009. JNK1-dependent PUMA expression contributes to hepatocyte lipoapoptosis. *J. Biol. Chem.* **284:** 26591–26602.

28. Kleiner, D. E., E. M. Brunt, M. Van Natta, C. Behling, M. J. Contos, O. W. Cummings, L. D. Ferrell, Y. C. Liu, M. S. Torbenson, A. Unalp-Arida, et al. 2005. Design and validation of a histological scoring system for nonalcoholic fatty liver disease. *Hepatology.* **41:** 1313–1321.

29. Malhi, H., F. J. Barreyro, H. Isomoto, S. F. Bronk, and G. J. Gores. 2007. Free fatty acids sensitise hepatocytes to TRAIL mediated cytotoxicity. *Gut.* **56:** 1124–1131.

30. Rutkowski, D. T., J. Wu, S. H. Back, M. U. Callaghan, S. P. Ferris, J. Iqbal, R. Clark, H. Miao, J. R. Hassler, J. Fornek, et al. 2008. UPR pathways combine to prevent hepatic steatosis caused by ER stress-mediated suppression of transcriptional master regulators. *Dev. Cell.* **15:** 829–840.

31. Scheuner, D., B. Song, E. McEwen, C. Liu, R. Laybutt, P. Gillespie, T. Saunders, S. Bonner-Weir, and R. J. Kaufman. 2001. Translational control is required for the unfolded protein response and in vivo glucose homeostasis. *Mol. Cell.* **7:** 1165–1176.

32. Hanada, K. 2003. Serine palmitoyltransferase, a key enzyme of sphingolipid metabolism. *Biochim. Biophys. Acta.* **1632:** 16–30.

33. Maceyka, M., and S. Spiegel. 2014. Sphingolipid metabolites in inflammatory disease. *Nature.* **510:** 58–67.

34. Kunkel, G. T., M. Maceyka, S. Milstien, and S. Spiegel. 2013. Targeting the sphingosine-1-phosphate axis in cancer, inflammation and beyond. *Nat. Rev. Drug Discov.* **12:** 688–702.

35. Volmer, R., K. van der Ploeg, and D. Ron. 2013. Membrane lipid saturation activates endoplasmic reticulum unfolded protein response transducers through their transmembrane domains. *Proc. Natl. Acad. Sci. USA.* **110:** 4628–4633.

36. Wang, G., M. Dinkins, Q. He, G. Zhu, C. Poirier, A. Campbell, M. Mayer-Proschel, and E. Bieberich. 2012. Astrocytes secrete exosomes enriched with proapoptotic ceramide and prostate apoptosis response 4 (PAR-4): potential mechanism of apoptosis induction in Alzheimer disease (AD). *J. Biol. Chem.* **287:** 21384–21395.

37. Costa-Silva, B., N. M. Aiello, A. J. Ocean, S. Singh, H. Zhang, B. K. Thakur, A. Becker, A. Hoshino, M. T. Mark, H. Molina, et al. 2015. Pancreatic cancer exosomes initiate pre-metastatic niche formation in the liver. *Nat. Cell Biol.* **17:** 816–826.

38. Kasumov, T., L. Li, M. Li, K. Gulshan, J. P. Kirwan, X. Liu, S. Previs, B. Willard, J. D. Smith, and A. McCullough. 2015. Ceramide as a mediator of non-alcoholic Fatty liver disease and associated atherosclerosis. *PLoS One.* **10:** e0126910.

39. Povero, D., A. Eguchi, H. Li, C. D. Johnson, B. G. Papouchado, A. Wree, K. Messer, and A. E. Feldstein. 2014. Circulating extracellular vesicles with specific proteome and liver microRNAs are potential biomarkers for liver injury in experimental fatty liver disease. *PLoS One.* **9:** e113651.